Observations of Saharan Aerosols: Results of ECLATS Field Experiment. Part I: Optical Thicknesses and Aerosol Size Distributions

Y. FOUQUART, B. BONNEL, M. CHAOUI ROQUAI AND R. SANTER

Université des Sciences et Techniques de Lille, Laboratoire d'Optique Atmosphérique, France

A. CERF*

Université d'Abidjan, Laboratoire de Physique de l'Atmosphère, 04 BP 4322 Abidjan, Côte d'Ivoire

(Manuscript received 2 December 1985, in final form 1 July 1986)

ABSTRACT

A series of ground-based and airborne observations of desert aerosols, the ECLATS[1] experiment, was carried out in December 1980 in the vicinity of Niamey (Niger). This paper deals with aerosol optical thicknesses and size distributions derived from (i) in situ measurements using single particle optical counters (a Kratel and a Knollenberg FSSP), (ii) a ground-based cascade impactor, and (iii) ground-based measurements of the spectral variation of the solar extinction.

During the experiment, aerosol optical thicknesses (at 550 nm) varied from 0.20 on very clear days to 1.5 during a so-called "dry haze" episode.

Comparisons between size distributions derived from in situ measurements from ground-based cascade impactor, and from inversion of the spectral optical thicknesses, showed that the optical counters drastically underestimated the concentration of small ($r < 0.5$ μm) particles. It was shown that the occurrence of a "dry haze" episode was characterized by a large increase (an order of magnitude in this particular case) of the intermediate particles ($r \cong 0.5$ μm), whereas the concentration in very small ($r < 0.2$ μm) and large ($r > 1$ μm) particles remained roughly constant.

1. Introduction

Through their interactions with both solar and terrestrial radiation, atmospheric aerosols can alter significantly the radiative budget of the earth–atmosphere system. In shortwaves, they reflect back to space a part of the incoming solar radiation and absorb another part of it, which results in a net decrease of the available solar energy at the earth's surface and a heating of the atmosphere. In the infrared, the increased atmospheric opacity induces an enhanced greenhouse effect. The net effect on the radiative budget depends upon the nature and size of the aerosols concerned, and also the surface albedo and the altitude of the aerosols layers.

The climatic effect of aerosols has been a subject of concern for several years. Particular attention has been given to stratospheric aerosols which reside long enough to significantly alter the climate. Many papers have dealt with the relationship between fluctuations in climate and volcanic activity through the interactions of injected stratospheric aerosols with radiation (Oliver, 1976, Pollack et al., 1976, Fiocco et al., 1976, Luther, 1976, Mass and Schneider, 1977, Lenoble et al., 1982). Attention has also been paid to tropospheric aerosols by Rasool and Schneider, 1971; Atwater, 1970; Chylek and Coakley, 1974; Harshvardhan and Cess, 1978; Hansen et al., 1978; Murray and Mitchell, 1971; Tanré et al., 1983; and Reck, 1976.

Actually, the insoluble particles produced by soil erosion constitute 10 to 20% of the total aerosol production rate (WCP 12 Report on aerosol and Climate, 1980). The tropical arid zones constitute the main source for these particles, and of these the Saharan and its bordering regions are certainly the most efficient.

In this context the so-called "dust hazes," which are a common feature of the countries bordering the Sahara, call for particular attention, as they might be related to the droughtness of Sahelian regions. Indeed, Prospero et al. (1972) noticed that an intense period of drought coincided with an abnormally high frequency of dust hazes. The problem is quite similar to that presented by the increased incidence of aerosols during the last ice age; namely, to determine whether aerosols induce a positive feedback on the desertification process through stabilizing processes in the boundary layer.

The development of dust hazes depends upon ITCZ position and North African high pressure systems whose speedy progress from northwest to southeast

* Present affiliation: Université des Sciences et Techniques du Languedoc—Laboratoire d'infrarouge—34060 Montpellier Cedex, France.

[1] Etude de la Couche Limite Atmosphérique Tropicale Sèche.

stimulates propitious conditions for their deflation, lifting enormous masses of aerosols into the atmosphere. The sources of aerosols are chiefly the Tchad's reservoir and Air's alluvia spurs. Dust is transported by the general circulation of the lower troposphere (below 600 mb). In these layers the residence time of the particles is considerably increased by the turbulence induced by high ground temperatures. The ITCZ constitutes a southern limit for aerosol-laden air masses, and its position affects the trajectory of dust hazes. In the Northern Hemisphere summer, when the ITCZ reaches high latitudes, they are directed towards Mauritania and Senegal, and Saharan aerosols are often transported through the Atlantic (Prospero and Carlson, 1972). In winter, the ITCZ is much further to the south and Harmattan winds transport Saharan aerosols towards the Guinea Golf, whereas in spring the ITCZ has an intermediate position which allows transport of aerosols above the north equatorial Atlantic towards Central America and the north of South America. Prospero et al., (1981) reported on observations of Saharan aerosols in French Guyana.

The spatial extension and the high frequency of occurrence of dust hazes is such that they can have a significant effect on the global climate through their impact on the radiative budget of the earth–atmosphere system. On the regional scale, in Sahelian regions they may induce a large dynamic effect by heating the atmosphere and cooling the surface, thus stabilizing the temperature lapse rate (Carlson and Benjamin, 1980). In order to evaluate this possible climatic impact, one needs to know the spatial and temporal extension of dust hazes, the concentration and optical properties of Sahelian aerosols, and the synoptic conditions associated with dry haze. The spatial and temporal extension of dust hazes can only be inferred from satellite measurements associated with well-defined ground truth measurements. Field experiments are needed not only as validations but also as they constitute the only way of measuring such parameters as the size distribution or chemical composition of aerosols which are not yet measurable from satellites. Field experiments also allow a direct experimental approach to evaluating the impact of aerosols on the dynamics of the lower atmosphere.

In November–December 1980, the Universities of Toulouse and Lille (Druilhet and Tinga, 1982; Druilhet and Durand, 1984) conducted a field experiment in Niamey (Niger). The ECLATS experiment (Etude de la Couche Limite Atmosphérique Tropicale Sèche) was designed to study the properties of a clear boundary layer in which radiative effects constitute an important factor of the energy budget.

The complete experiment included in situ measurements of turbulence, radiative fields, aerosol concentrations and size distributions, as well as mesoscale observations of wind velocity and radiosounding (in Niamey). An aircraft (HD 34 INAG-EDF) was operated, fully instrumented with gust probes, inertial platform, Eppley pyranometers and pyrgeometers, Barnes PRT 5 radiometers, Knollenberg FSSP probe and a Kratel optical counter. A ground station was equipped with a Sierra Instruments cascade impactor, Eppley pyranometers and pyrgeometers and two interference filters sun photometers developed at LOA (giving measurements of the spectral extinction from 0.45 to 2.2 μm). A tethered balloon was also operated between the ground and 500 m to study the characteristics of the nocturnal boundary layer (Guedalia et al., 1984). One of the main objectives of ECLATS was to determine the radiative properties of the Saharan aerosols during the Northern Hemisphere winter and their impact on the radiative field.

This paper (Part I) reports on measurements of the extinction optical depths made during ECLATS and deduced size distributions. In situ measurements made on board the HD-34 instrumented aircraft are also reported.

Part II of this report (Fouquart et al., 1986) deals more specifically with the determination of the short wave single scattering albedo and infrared emissivity of aerosols, and reports on observations of longwave and short wave radiative fluxes and corresponding heating rates.

2. Observations of solar extinction

The meeting of JSC experts on aerosols and climate (WCP 12, 1980) emphasized the need for turbidity measurements, particularly around the major sources of desert aerosols. Though the accuracy of turbidity measurements is crucially dependent on the frequency of inspections and recalibration procedures, they constitute a useful tool (as well as a cheap one) for continuous monitoring of the global aerosol loading in the atmosphere. Well-calibrated pyrheliometers or sun photometers constitute the necessary ground truths for satellite measurements; moreover the determination of aerosol optical thickness at suitable wavelengths gives insight into aerosol size distributions.

Optical thickness (δ) of Saharan dust has been determined by a number of authors from turbidity measurements. Cerf (1980) observed, in Niger and upper Volta, values up to 0.8, at λ = 506 nm, whereas in Cape Verde Islands during the GATE observational programme in 1974, Carlson and Caverly (1977) observed averaged values of optical thickness around 0.9 to 1.0 for the haziest days and around 0.5 for the remaining days. The sun photometer measurements program, coordinated by Prospero et al. (1979), allowed construction of a mean dust plume map with seasonal averaged optical thickness, ranging from 0.3 along the coast of Africa to 0.1 in the western Atlantic.

Observations of solar extinction are also available from the Middle East, where the Khamsinic conditions correspond to advection from desert areas so that large

TABLE 1. Central wavelength (λ) and spectral bandpass (Δλ) of the multiwavelengths radiometers used during ECLATS.

	Radiometer 1							Radiometer 2			
	1	2	3	4	5	6	7	1	2	3	4
λ (nm)	443	525	550	600	678	336	338	865	1040	1580	2210
Δλ (Å)	155	80	85	100	70	17	36	25	30	55	72

quantities of saharan dust are transported up to Lebanon and Syria; Levin et al., (1980) reported a maximum optical thickness of roughly 2, peaking to 3 just after a frontal passage. According to Levin et al., for averaged Khamsinic conditions the optical thickness would be around 1.5.

a. Instruments and measurements

Two multiwavelength filter wheel radiometers constructed at Laboratoire d'Optique Atmosphérique de Lille were available for ECLATS. They differed in their detectors and apertures. The first one, with a Silicium detector, covered the range from 400 to 1100 nm with a 3° field of view, whereas the second one, with a PbS detector, covered the near infrared from 800 to 3000 nm with a field of view of 5°. The bandpass of the interferometer filters is summarized in Table 1. Note that channels 6 and 7 were used to determine the water vapor content (not discussed here).

Neglecting the small contribution of the multiple scattering which occurs within the field of view of the radiometer, the directly transmitted solar irradiance $I(\lambda)$ is given by

$$I(\lambda) = I_o(\lambda) \exp[-m\delta(\lambda)] \quad (1)$$

where $I_o(\lambda)$ is the solar irradiance at the top of the atmosphere, $\delta(\lambda)$ the optical thickness at wavelength λ, and m is the air mass depending on the solar zenith angle θ_o. The $\delta(\lambda)$ represents total extinction, including molecular scattering $\delta_R(\lambda)$, molecular absorption $\delta_g(\lambda)$ and aerosol extinction $\delta_A(\lambda)$:

$$\delta(\lambda) = \delta_R(\lambda) + \delta_g(\lambda) + \delta_A(\lambda).$$

Radiometer calibration was derived from the usual Langley plot method. Typically 40 data points were used. On some occasions the presence of thin cirrus clouds was detected, or the aerosol content of the atmosphere changed during the period when measurements were being taken; in these cases, the values of $\delta(\lambda)$ recorded relate to the period of the day during which conditions were stable.

The near-infrared channels were chosen in the atmospheric windows; however, measurements recorded on channel 4 of radiometer 2 have been disregarded as that channel probably was contaminated by water vapor absorption. The scattering optical depth $\delta_R(\lambda)$ for the molecular atmosphere was obtained with the help of tables and surface pressure measurements. Ozone absorption was calculated by means of the

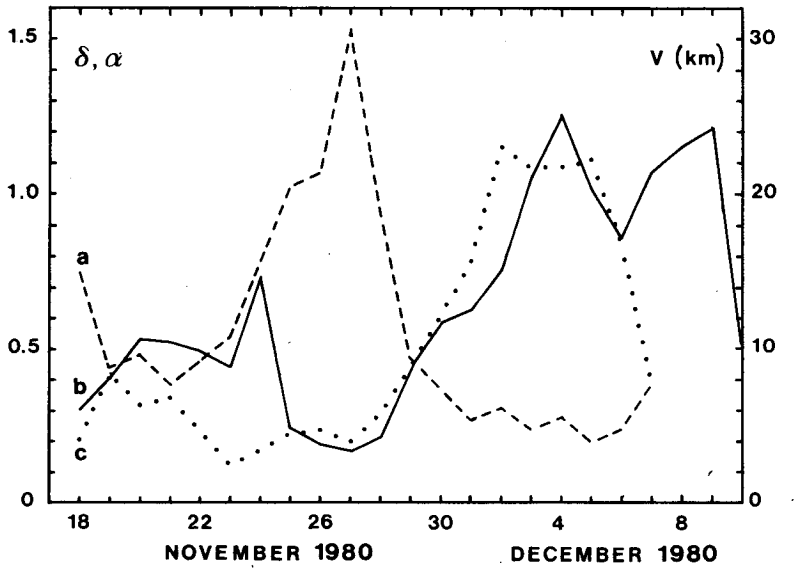

FIG. 1. Optical depth δ at λ = 520 nm (curve a, dashed line), horizontal visibility V (curve b, solid line) and Angström coefficient α (curve c, dotted line) for the period of ECLATS Experiment.

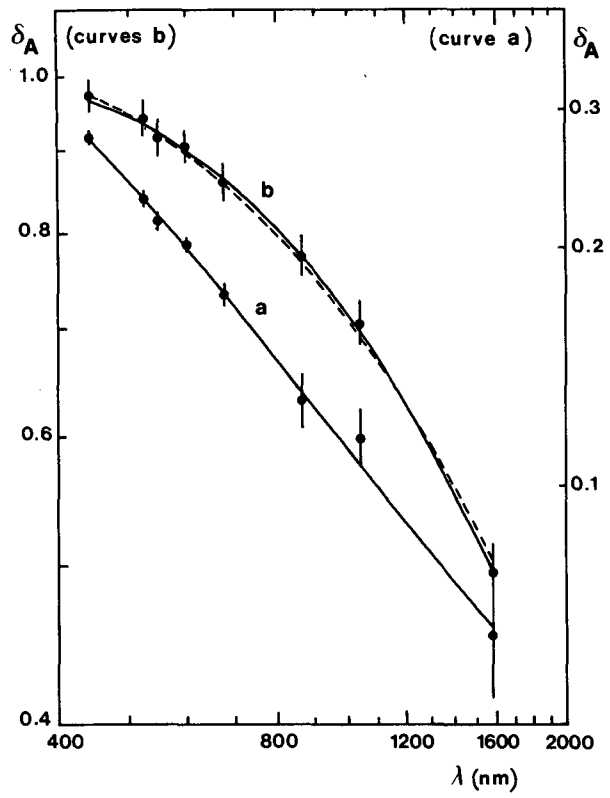

FIG. 2. Spectral variation of the aerosol optical thickness δ_A for clear sky (curve a: 3 December 1980) and hazy sky (curve b: 28 November 1980); reported values are at λ = 443–525–550–600–678–865–1040–1580 nm. Error bars correspond to the dispersion around the Bouguer plot. Continuous curves: optical thicknesses computed with a size distribution deduced from King's method (solid lines), and Box's method (dashed line).

LOWTRAN 5 program (Kneizys et al., 1980) using the ozone climatological data.

b. *Observations*

Figure 1 represents optical thickness at 520 nm and horizontal visibility in Niamey for the period of the ECLATS experiment. A moderate dry haze occurred from 23 to 28 November, with optical depths reaching 1.5 on the twenty-seventh, in good agreement with the just mentioned observations. It is interesting to note that a very intense dry haze occurred a short time after the end of ECLATS; turbidity measurements were no longer available at that time, but horizontal visibility decreased to less than 500 m.

Figure 2 shows the spectral variation of the aerosol optical thickness $\delta_A(\lambda)$ for the two extreme—clear and hazy—cases. The error bars correspond to the dispersion around the Bouguer plot, and include the radiometric noise as well as the natural variability of aerosols. [Solid curves represent $\delta_A(\lambda)$ recomputed via Eq. (2) with a size distribution deduced from inversion methods—see section 3]. At first sight, the main difference between the two curves lies in their concavity which changes from clear to hazy conditions; these results will be analyzed thoroughly in section 3. A second interesting point is that most of these curves are not linear in this log–log diagram. Consequently, the usual Angström presentation [$\delta(\lambda) = \beta \cdot \lambda^{-\alpha}$] is unable to restitute the complete spectral variation of δ; however, as many results are still presented using this presentation, the daily variation of the Angström exponent α is also presented in Fig. 1. For consistency with other published results α was derived from the visible spectral range ($\lambda < 700$ nm). It is interesting to note that, in agreement with the previous statement on Fig. 2, large δ are associated with small α (roughly $\alpha \approx 0.2$), while for the clearest days α reaches its standard continental value ($\alpha \approx 1.3$). Since α is approximately related to the exponent ν of a Junge distribution ($dN/dr \approx r^{-(\nu+1)}$ with $\nu = \alpha + 2$), such a variation denotes a significant change in size distribution with a shift toward larger particles for the haziest days.

3. Size distributions

Direct measurements of aerosol size distributions were performed during ECLATS: at ground level by means of a cascade impactor (from Sierra Instruments Co.) and in situ, from the aircraft, by means of a Knollenberg FSSP and a single particle counter Kratel, which is quite similar to a Royco 220. Table 2 summarizes the size discretization of the three instruments. In addition, the ground-based spectral solar extinction measurements have been inverted to restitute the integrated size distributions. This section presents the results of these measurements and the observed differences are discussed.

a. *Inversion of spectral optical thicknesses*

For spherical particles, the aerosol optical thickness is related to the size distribution by

$$\delta_A(\lambda) = a \int_0^\infty \pi r^2 Q_{\text{ext}}(r/\lambda, \tilde{m}) \bar{n}(r) dr \qquad (2)$$

where $\bar{n}(r)$, normalized to a single particle, is the size distribution integrated over the whole vertical atmospheric column, a the total number of particles in this

TABLE 2. Size discretization of classes for cascade impactor, Knollenberg FSSP and Kratel counters.

	Number of classes	radii (μm)
Cascade impactor	6	<0.15; 0.15–0.30; 0.30–0.60; 0.60–1; 1–2.5; >2.5
Knollenberg	16	regularly spaced from 0.25 to 4 μm, with Δr = 0.25 μm
Kratel	5	0.225–0.25; 0.25–0.7; 0.7–1; 1–1.5; 1.5–5.5

vertical column, and $\pi r^2 Q_{ext}$ the extinction cross section, which is here calculated from Mie theory with the complex refractive index $\tilde{m}$ from Patterson et al. (1977) or Carlson and Benjamin (1980) (i.e., $\tilde{m} = 1.55 - 0.005i$).

Generally two kinds of inversion are available: the analytical method with an assumed size distribution, and the direct linear method. Calculations using both methods are performed hereunder.

1) Analytical inversion (improved Box's method)

Inversion of the spectral variation of $\delta_A(\lambda)$ is easier if $n(r)$ is a simple analytic function of r. For measurements restricted to the visible range (443–678 nm), the spectral dependance of $\delta_A(\lambda)$ is reasonably approximated by the Angström formulation $\delta_A \approx \lambda^{-\alpha}$, the inversion of which gives the well-known Junge distribution $n(r) \approx r^{-(\alpha+3)}$. As noted by Deirmendjian (1980), that simplicity is only apparent since the lower (r_1) and upper (r_2) limits of the inversion need to be fixed. We preferred to use the gamma-standard law

$$\bar{n}(r) = cr^{(1-3v)/v} \exp(-r/rv) \qquad (3)$$

where c is a normalized constant, r the effective radius, and v the effective variance. With measurements restricted to the visible, the inversion is limited to a single parameter, r, and the variance is arbitrarily fixed to $v = 0.2$ (Box and Lo, 1976). By extending the measurements to the near infrared and noting that there is a change in the slope of δ vs λ (see Fig. 2), it appears feasible to determine v also. The determination of r and v is done using a grid point method which minimizes the distance between precalculated and observed Angström exponents α_V and α_{IR}. Observed Angström exponents α_V and α_{IR} are obtained from a least-square fitting to the spectral extinction measurements of radiometer 1 (443–678 nm) and 2 (865–1580 nm), respectively; the total number of particles a is derived from Eq. (2).

One advantage of this method is that in the analytical form of the distribution, which facilitates the modelization, the two parameters r and v allow classification between different aerosol models. The choice of the distribution law is, obviously, arbitrary; however, Küriyan et al. (1974a,b) showed that the gamma standard law with a single variable parameter r ($v = 0.2$) was able to describe the radiative effects of Deirmendjian's hazes H, L and M in the visible. Thus, one can reason that with a second variable parameter (v), the domain of validity of the gamma standard law extends to the near infrared. Similarly, Lenoble and Brogniez (1983), for the standard radiation atmospheres, showed that gamma standard and log-normal laws are equivalent. Nevertheless, this type of analytical distribution has limitations; in particular in the case of multimodal distributions, the gamma standard law is deficient.

2) Linear inversion (King's method)

Due to these limitations in the analytical inversion method, we also applied the constrained linear inversion method. This method, which is fully described in King et al. (1978) and King (1982), does not prescribe an analytical form $\bar{n}(r)$ and can be used even for multimodal distributions. The dataset for the inversion includes measurements at eight wavelengths (443, 525, 550, 600, 678, 865, 1040 and 1580 nm). The lower limit of detectability is set to $r_1 = 0.1$ μm, since smaller particles have a negligible impact on the signal. On the other hand, since the extinction efficiency oscillates around $Q_{ext} \approx 2$ for $x = 2\pi r/\lambda \geqslant 15$, large particles are undetectable; with $\lambda \approx 1600$ nm, the upper limit settles to $r_2 \approx 4$ μm; the seven classes of the inverted size distributions are centered at 0.14, 0.23, 0.39, 0.65, 1.10, 1.88 and 3.2 μm, respectively.

Both methods have been applied to the measurements presented in Fig. 2. The restituted spectral variations are reported in the figure for both methods for the haziest day, whereas for the clear case, due to the concavity of $\delta_A(\lambda)$, Box's method does not apply. The corresponding inverted size distributions are presented on Fig. 3, showing for the hazy case a reasonable agreement between the two methods. Error bars on this figure were obtained following King (1982); the greatest uncertainties arise for large particles, for which the in-

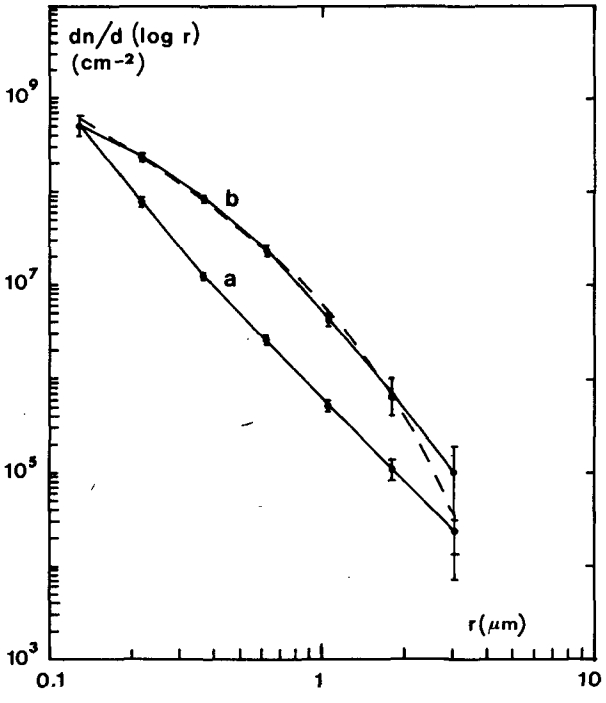

FIG. 3. Aerosol size distributions integrated over the whole atmospheric column corresponding to the spectral optical thicknesses showed in figure 2, derived from constrained linear inversion (solid lines), and Box's method (dashed line). Curve a: 3 December 1980; curve b: 28 November 1980.

formation content of the spectral extinction is the smallest. As the complete spectral variation of $\delta_A(\lambda)$ includes measurements from two different radiometers, intercalibration problems lead to an additional uncertainty for King's method. Intercalibration was possible as the spectral range of the two radiometers overlap around 900 nm; in addition, as Box's method depends only on Angström exponents which are derived independently for each radiometer, the good agreement between the two-inverted size distribution and the good restitution of the spectral variation of $\delta_A(\lambda)$ indicates that the intercalibration is satisfactory. In the following we use the constrained linear inversion method which applies for all cases, even clear ones where Box's method fails, because the gamma standard law is not representative of the actual size distribution.

b. Observations

Direct observations of the aerosol size distribution on 18 November are presented in Fig. 4. For consistency with ground-based impactor measurements, the reported aircraft observations (Kratel and Knollenberg) were collected during low-level flights performed at an altitude of roughly 100 m. Kratel and Knollenberg distributions are local and instantaneous measurements, whereas the cascade impactor distributions correspond to an average over 24 h; however, both aircraft measurements showed only small variations in the distribution over the 24 h period. The distributions derived from ground-based extinction measurements are given for the corresponding 2 days and are not very different. These last results are integrated over the whole atmospheric column; however, aircraft measurements show a fair stability of the distributions with height, as shown in Table 3, which gives the distributions normalized to the concentration in the first class of the Kratel for different altitudes. Although significant, the variations remain smaller than a factor of 2; the Knollenberg distributions have not been reported as they are almost invariant. These preliminary discussions validate the intercomparisons, at least for relative abundances, between the different size distributions.

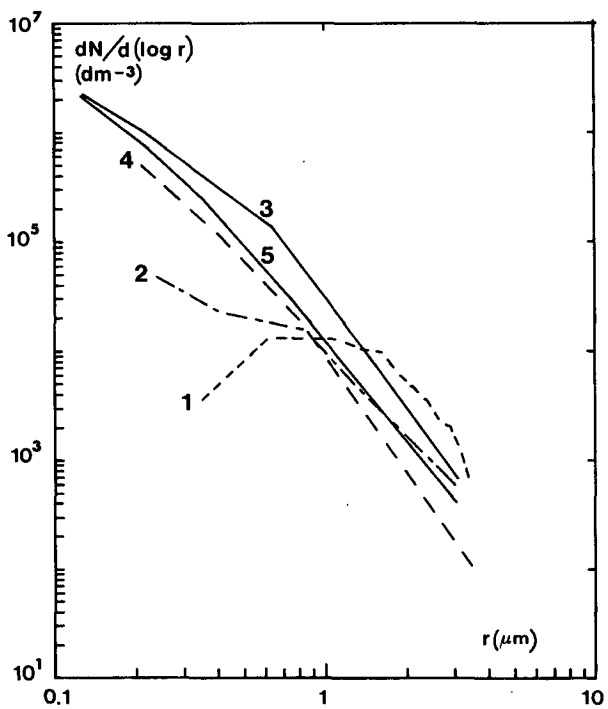

FIG. 4. Aerosol size distributions observed during ECLATS (day: 18 November 1980) from four different methods: curves 1 and 2, direct in situ (low level flight) optical counters (Knollenberg and Kratel, respectively); curve 3, derived from spectral extinction measurements; and curve 4, ground based cascade impactor; curve 5, same as curve 3 but for the 19 November data.

TABLE 3. Dependance of normalized size distributions with the altitude $(dN/d\ \log r)_{\text{class } i}/(dN/d\ \log r)_{\text{class } 1}$.

	Altitude (ft)			
Class (μm)	100	1500	3000	5300
0.225–0.25	1	1	1	1
0.25–0.70	0.77	0.73	0.74	0.74
0.70–1.0	1.40	1.27	1.11	1.01
1.0–1.5	0.75	0.68	0.50	0.41

Impactor and inversion measurements lead to good agreement. But, except for large particles, both Kratel and Knollenberg results disagree with these size distributions. Note that for $r = 0.2$ μm Kratel and Knollenberg already differ by almost one order of magnitude. Since the accuracy of the inversion strongly decreases for large particles as the information content of $\delta_A(\lambda)$ is weak (see the error bars in Fig. 3), the very nice agreement for $r > 1$ μm must be taken with caution.

Independent of the method used to invect the spectral inversion measurements, the experimental size distributions, once vertically integrated, should lead to a reasonable qualitative agreement between the observed spectral variation of $\delta_A(\lambda)$ and the recalculated one. However, this is not the case, as may be seen in Fig. 5 where the optical thicknesses recomputed via the Mie's theory for the vertically integrated Knollenberg (curve 1) and Kratel (curve 2) distributions are compared to the measured $\delta_A(\lambda)$ and the values recalculated from the inverted size distribution (curve 3). The disagreement is also very clear in Fig. 6 where the integrated size distributions are shown, derived from the constrained linear inversion and from vertically integrated in situ measurements: for the smallest detectable particles ($r \simeq 0.2$ μm), the discrepancy reaches one order of magnitude with the Kratel and two orders with the FSSP.

We were unable to determine the precise cause of such a large discrepancy; however according to Jeck (1979), two reasons could be proposed for underesti-

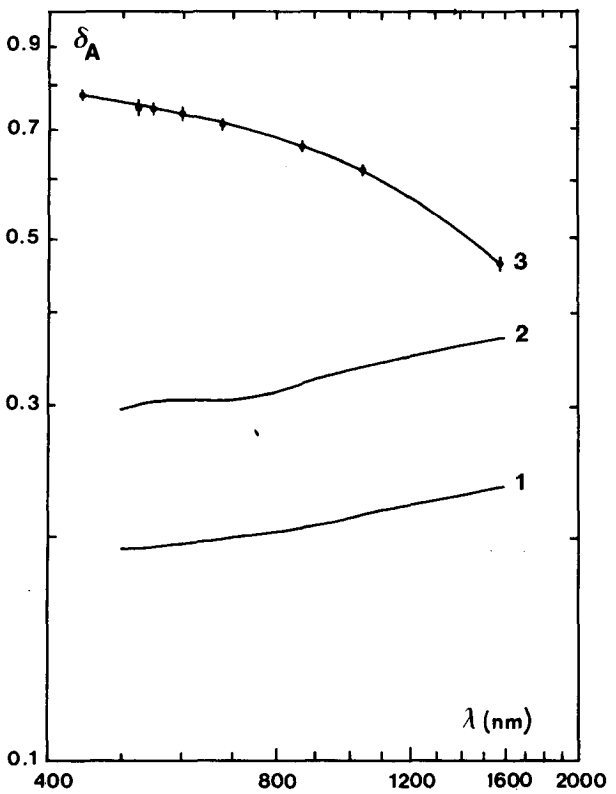

FIG. 5. Comparison between $\delta_A(\lambda)$ recomputed from 1) Knollenberg measurements; 2) Kratel measurements; and 3) results of constrained linear inversion. Day: 18 November 1980. See Fig. 6 for corresponding size distributions.

mating the number of small particles with the FSSP: (i), a saturation of particle count, due to an improper circuit response time associated with the finite dead time following the transit of a particle; however, the maximum rate of small detectable particles is roughly 6000 s^{-1} according to ground-based optical measurements, far less than the 100 000 particles per second which correspond to the dead time of 10 s; (ii), side effects of the edge rejection circuitry; however, according to Particle Measuring System, the edge rejection circuitry is not supposed to cause any spectral distortion in the measurement of clear air aerosols.

According to Whitby and Willeke (1979), a random generation of countable pulses by subcountable size particles tends to occur with the Royco, resulting in a decrease of one or two orders of magnitude in the lowest channel and an increase in the larger sizes. According to ground-based optical measurements, the rate of particles with $r < 0.1$ μm would be 100 000 to 130 000 particles per second for the FSSP; it might be that a similar noise generation occurs with the FSSP.

The cascade impactor itself can be affected by reentrainment of large particles resulting in a large overestimate of small particles, whereas the inversion of spectral extinction is known to be inaccurate for large particles, though measurements of δ in the near infrared considerably improve the accuracy of the inversion.

In any case, the main objective of the present study is the determination of the radiative effects of the Saharan aerosols. In this respect, the inconsistency of the results presented in Fig. 5 (observed spectral variation of the optical thickness and calculated assuming the size distributions measured by the optical counters) is definitely not unacceptable. We thus choose to use the distributions derived from the spectral extinction measurements for analyzing the remaining radiation observations. Despite their uncertainty in large particle concentration, it will be shown in Part II of this study that these distributions allow a realistic characterization of the radiative properties of the Saharian aerosols.

The size distributions presented in Fig. 3 for a typical clear day (3 December) and a hazy day (28 November), show that the dry haze is characterized by a large increase (about a factor of 10) in the number of particles of intermediate size, whereas the occurrence of small and large particles remains nearly unchanged. This is consistent with the idea of a background of small particles which constitute a permanent feature in West Africa, the dry haze itself being mostly constituted of intermediate particles ($r = 0.5$ μm). The small variation in the concentration of large particles ($r > 2$ μm) might be related to a decantation process, large particles being mostly of local origin.

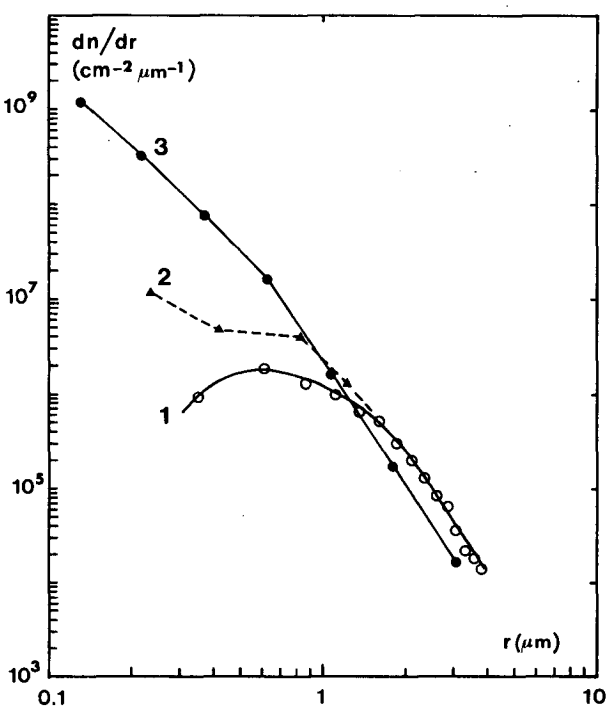

FIG. 6. Vertically integrated aerosol size distributions obtained from 1) Knollenberg measurements; 2) Kratel measurements; and 3) constrained linear inversion. Day: 18 November 1980.

Extensive measurements of Saharan dust size distributions are available for comparison with our results. In Fig. 7 we have drawn the distribution characteristics of hazy conditions during ECLATS (curve 1), which can be compared with size distributions determined over the eastern Atlantic during GATE (curve 2): Kondrat'yev et al., 1981 (curve 3): Jaenicke and Schütz, 1978 (curve 4): Carlson and Caverly, 1977. Measurements made in Senegal are represented by curve 5 (d'Almeida and Jaenicke, 1981); the distribution observed in Khamsin conditions (Levin et al., 1980) is also shown (curve 6), as well as the continental II aerosol distribution (curve 7) of the Standard Radiation Atmosphere (WCP 12, 1980). Although discrepancies between individual curves are large some similarities can be drawn: all distributions except Kondrat'yev et al. give roughly a similar slope for large particles ($r > 1$ μm), viz. $\alpha \approx 2.3$, whereas for SRA, $\alpha \approx 3$. The main discrepancy occurs in the intermediate range (0.1 μm $\leq r \leq 1$ μm) where most authors conclude there is a much smaller slope than was obtained from ECLATS (Carlson and Caverly: $\alpha \approx 1$, d'Almeida and Jaenicke: $\alpha \approx 0.5$) or to an important decrease (Levin et al., Kondrat'yev et al.). According to Jaenicke (1982) and Kondrat'yev et al. (1982), the gap in intermediate particles observed in curve 2 is certainly unrealistic, at least for its magnitude. The slope of the ECLATS distribution remains close to 2 for $r > 0.3$ μm while Jaenicke's slope is intermediate. The SRA Continental II has the strongest slope ($\alpha \approx 3$). For the smallest particles there is fairly good agreement among the distributions, most giving a high relative concentration of small particles except Levin et al. (1980) and, to a lesser extent, Carlson and Caverly (1977). According to Levin et al., the wind speed at the time of the frontal passage exceeded 10 m s^{-1}, whereas during ECLATS it was always smaller than 4 m s^{-1}. As suggested by Levin et al., this wind speed might explain an important local generation of large particles in Khamsin, whereas this generation was small during ECLATS. As for the SRA, it can be seen that the small particles are overwhelmingly water soluble ($\alpha \approx 3.4$ and the relative concentration in terms of particle number $\approx$94%) and that is probably not appropriate for desert aerosols.

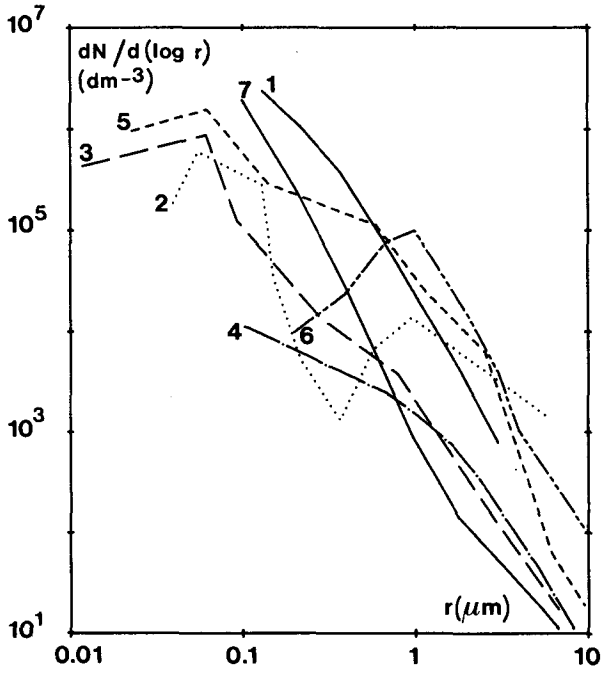

FIG. 7. Comparison between a typical aerosol size distribution observed during ECLATS Experiment (curve 1), and those done by other authors: curve 2, Kondrat'yev et al. (eastern Atlantic); curve 3, Jaenicke and Schütz; curve 4, Carlson and Caverly; curve 5, D'Almeida and Jaenicke (Senegal); curve 6, Levin et al. (Khamsin conditions); and curve 7, Standard Radiation Atmosphere.

4. Summary and conclusions

Large concentrations of saharan aerosols were observed during the ECLATS fields experiment (Niger, November–December 1980). At the time of a "dry haze", the aerosol optical thickness rose to $\delta_A = 1.5$ at $\lambda = 520$ nm. Airborne measurements of aerosol size distribution were obtained by means of single particle optical counters Kratel and Knollenberg FSSP (SPOC); simultaneously, size distributions were obtained from ground-based measurements using a cascade impactor, and inversions of spectral extinction measurements led to vertically integrated size distributions. Two methods of inversion were used: the first is an extension of the Box and Lo (1976) method, while the second is the constrained linear inversion method developed by King et al. (1978, 1982). Both methods lead to very similar results for hazy days.

The size distributions derived from the two SPOC differed very significantly from those derived from optical extinction measurements or from the cascade impactor. The good agreement between the cascade impactor and the spectral extinction data might be a coincidence, since cascade impactors are known to be subject to reentrainment which may lead to large overestimate of the small particles concentration. However, the distributions derived from the SPOC were unable to account for the observed aerosol radiative effects as will be reported in paper II, whereas the distributions derived from the spectral extinction measurements led to a fairly good agreement. Consequently we adopted the size distribution resulting from King's inversion method as representative of the actual distribution, at least for the purposes of analyzing the optical effects. It should be noted that this distribution may significantly differ from the actual unknown one; however, as it will be shown in a future paper, it has always agreed with all radiative measurements performed during ECLATS: shortwave and longwave radiative fluxes as well as infrared window radiances. We thus consider the assumed distribution to be representative

of some effective size distribution, the optical effects of which are similar to those of the actual one.

Comparison of in situ and ground-based measurements showed that both optical counters strongly underestimated the number of small particles ($r \leqslant 1$ μm). Reasons for this inaccuracy were not identified precisely, though they might be related to the noise generated by the large number of undetectable particles. Classical ground-based aureola measurements would have been useful for measuring the presence of large particles and are to be used for further studies. Similarly, polarization measurements would have been useful in deriving the particles refractive index.

Aerosol size distributions observed during ECLATS included a large concentration of relatively small particles ($r \leqslant 1$ μm); this contradicts the observations of some other authors (Carlson and Caverly, 1977; Kondrat'yev et al., 1981; or Levin et al., 1980) who observed small relative concentration of small particles. These differences are partly due to the methods of measurements themselves: most particle optical counters are unable to detect particles smaller than 0.2 μm in radius; also, as experienced during ECLATS, they can strongly underestimate the number of the smallest detectable particles. Our measurements showed a systematic decrease in particle concentration, with decreasing r for small particles ($r \leqslant 0.5$ μm) with the FSSP and a small increase with the Kratel; with a Knollenberg FSSP, Ackerman and Cox (1982) obtained roughly similar distributions over Saudi Arabia. Our spectral extinction measurements might lead to large uncertainties in the inverted size distributions, mainly for the largest particles, but the order of magnitude of the concentration of small particles given by the distributions is certainly more reliable, as is confirmed by the generally good agreement between our results and those collected by d'Almeida and Jaenicke (1982) or Jaenicke and Schütz (1978).

Discrepancies between observed relative concentrations of small particles are also related to differences in wind velocity, as large particles are mostly due to local generation. In this respect the "dry hazes" observed during ECLATS are characterized by small or moderate wind velocity ($V < 4$ m s^{-1}) as opposed to dust storm conditions or khamsin conditions. In addition, differences in origin and humidity conditions may strongly affect the size distribution.

This large relative concentration of small particles obviously has important consequences on the optical properties of the Saharian aerosols layer.

Acknowledgments. This work was supported by CNRS-INAG under contract of ATP Recherches Atmosphériques. The authors wish to express their deep gratitude to all of those who helped to make ECLATS a success, in particular Dr. Druilhet, who directed the study, the University of Niamey and the authorities of Niger for their active collaboration. They thank Professor Volz for providing the refractive indices in the infrared domain. Thanks are also due to J. C. Vanhoutte for his technical help during ECLATS and the postprocessing of the data, and to Y. Théroux for typing the manuscript.

REFERENCES

Ackerman, S. A., and S. K. Cox, 1982: The Saudi Arabian heat low. *J. Geophys. Res.*, **87**, 8991–9002.

Atwater, M. A., 1970: Planetary albedo changes due to aerosols. *Science*, **170**, 64–66.

Box, M. A., and S. Y. Lo, 1976: Approximate determination of aerosol size distributions. *J. Appl. Meteor.*, **15**, 1068–1076.

Carlson, T. N., and R. S. Caverly, 1977: Radiative characteristics of saharan dust at solar wavelengths. *J. Geophys. Res.*, **82**, 3141–3152.

——, and S. G. Benjamin, 1980: Radiative heating rates for Saharan Dust. *J. Atmos. Sci.*, **37**, 193–213.

Cerf, A., 1980: Atmospheric turbidity over West-Africa. To *Contributions Atm. Phys.*, **53**, 3, 414–429.

Chylek, P., and J. A. Coakley Jr, 1974: Aerosols and climate. *Science*, **183**, 75–77.

d'Almeida, G., and R. Jaenicke, 1981: The size distributions of mineral dust. *J. Aerosol Sci.*, **12**, 160–162.

Deirmendjian, D., 1980: A survey of light scattering techniques used in the remote monitoring of atmospheric aerosols. *Geophys. and Space Phys.*, **18**, 2, 341–360.

Fiocco, G., G. W. Grams and A. Mugnai, 1976: Energy exchange and temperature of aerosols in the earth's atmosphere. *J. Atmos. Sci.*, **33**, 2415–2424.

Druilhet, A., and A. Tinga, 1982: Presentation de l'expérience ECLATS. *Météorologie*, **29**, 203–212.

——, and P. Durand, 1984: Etude de la couche limite convective sahélienne en présence de brumes sèches (expérience ECLATS). *Bound. Layer. Meteor.*, **28**, 51–77.

Fouquart, Y., B. Bonnel, J. C. Brogniez, L. Buriez, L. Smith and J. J. Morcrette, 1986: Observations of Saharan Aerosols: Results of ECLATS field experiment. Part II: Broadband radiative characteristics of the aerosols and vertical radiative flux divergence. *J. Climate Appl. Meteor.*, **25**.

Guedalia, D., C. Estournel and R. Vehil, 1984: Effects of Sahel dust layers upon nocturnal cooling of the atmosphere (ECLATS Experiment). *J. Climate Appl. Meteor.*, **23**, 644–650.

Hansen, J. E., W. C. Wang and A. A. Lacis, 1978: Mount Agung provides test of a global climate perturbation. *Science*, **199**, 1065–1068.

Harshvardhan, and R. D. Cess, 1978: Effect of tropospheric aerosols upon atmospheric infrared cooling rates. *J. Quant. Spectrosc. Radiat. Transfer*, **19**, 621–632.

Jaenicke, R., 1982: Comment on "determination of vertical profiles of aerosol size spectra from aircraft radiative flux measurements, 1, retrieval of spherical particles size distributions" by Kondratyev et al. *J. Geophys. Res.*, **87**, 7347–7349.

——, and L. Schutz, 1978: Comprehensive study of physical and chemical properties of the surface aerosols in the Cape Verde Islands region. *J. Geophys. Res.*, **83**, 3585–3599.

Jeck, R. K., 1979: Performance of the PMS axially scattering spectrometer probe. Aerosol Measurement. University Press of Florida, 716 pp.

King, M. D., 1982: Sensitivity of constrained linear inversions to the selection of the Lagrange multiplier. *J. Atmos. Sci.*, **39**, 6, 1356–1369.

——, D. M. Byrne, B. M. Herman and J. A. Reagan, 1978: Aerosol size distributions obtained by inversion of spectral optical depth measurements. *J. Atmos. Sci.*, **35**, 2153–2167.

Kneizys, F. X., E. P. Shettle, W. O. Gallery, J. H. Chetwind Jr., L. W. Abren, J. E. A. Selby, R. W. Fenn and R. A. McClatchey, 1980: Atmospheric transmittance/radiance: Computer code LOWTRAN 5, Report AFGL-TR-80-0067, 233 pp.

Kondrat'yev, K. Ya., R. M. Welch, S. K. Cox, V. S. Grihechkin, V. A. Ivanov, M. A. Prokofyev, V. F. Zhavlev and O. B. Vasilyev, 1981: Determination of vertical profiles of aerosol size spectra. From aircraft radiative flux measurements; 1. Retrieval of spherical particles size distributions. *J. Geophys. Res.*, **86,** 9783–9793.

——, ——, ——, ——, ——, ——, —— and ——, 1982: Reply to comment of R. Jaenicke (1982). *J. Geophys. Res.*, **87,** 7349.

Kuriyan, J. G., and Z. Sekera, 1974: Scattering in liquid haze. Analytic approximations. *Quart. J. Roy. Meteor. Soc.*, **100,** 67–75.

——, D. H. Phillips and M. T. Chahine, 1974: Multispectral extinction measurements to deduce the complex refractive index and size distribution of aerosol particles. *J. Atmos. Sci.*, **31,** 2233–2236.

Lenoble, J., and C. Brogniez, 1983: A comparative review of radiation aerosol models. To *Contributions Atm. Phys.*

——, D. Tanre, P. Y. Deschamps and M. Herman, 1982: A simple method to compute the change in earth atmosphere radiative balance due to a stratospheric aerosol layer. *J. Atmos. Sci.*, **39,** 2565–2576.

Levin, Z. L., J. H. Joseph and Y. Mekler, 1980: Properties of Sharaw (Khamsin) dust comparison of optical and direct sampling data. *J. Atmos. Sci.*, **37,** 882–891.

Luther, F. M., 1976: Relative influence of stratospheric aerosols on solar and longwave radiative fluxes for a tropical atmosphere. *J. Appl. Meteor.*, **15,** 951–955.

Mass, C., and S. H. Schneider, 1977: Statistical evidence on the influence of simspots and volcanic dust on long-term temperature records. *J. Atmos. Sci.*, **34,** 1995–2004.

Murray M. J. Jr., 1971: The effect of atmospheric aerosol on climate with special reference to temperature near the earth's surface. *J. Appl. Meteor.*, **10,** 703–714.

Oliver, R. C., 1976: On the response of hemispheric mean temperature to stratospheric dust: an empirical approach. *J. Appl. Meteor.*, **15,** 933–950.

Patterson, F. M., D. A. Gillette and B. H. Stockton, 1977: Complex index of refraction between 300 and 700 nm for Saharan aerosols. *J. Geophys. Res.*, **82,** 21, 3153–3160.

Pollack, J. B., O. B. Toon, C. Sagan, A. Summers, B. Baldwin and W. VAN CAMP, 1976: Volcanic explosions and climatic change. *J. Geophys. Res.*, **81,** 1071–1083.

Prospero, J., and T. N. Carlson, 1972: Vertical and areal distribution of saharan dust over the Western Equatorial North Atlantic Ocean. *J. Geophys. Res.*, **77,** 5255–5265.

Prospero, J. M., D. L. Savoie, T. N. Carlson and R. T. Nees, 1979: Monitoring Saharan aerosol transport by means of atmospheric turbidity measurements. *M.C. Morales—Saharan dust—SCOPE 14,* 297 pp.

——, R. A. Glaccum and R. T. Nees, 1981: Atmospheric transport of soil dust from Africa to South America. *Nature,* **289,** 570–572.

Rasool, S. I., and S. H. Schneider, 1971: Atmospheric carbon dioxide and aerosols: effects of large increases on global climate. *Science,* **173,** 138–141.

Reck, R. A., 1976: Thermal and radiative effects of atmospheric aerosols in the northern hemisphere calculated using a radiative convective model. *Atmos. Environ.*, **10,** 611–617.

Tanre, D., J. F. Geleyn and J. Slingo, 1983: First results of the introduction of an advanced aerosol radiation interaction in the ECMWF low resolution global model. *Proceedings of the workshop on Aerosols and their Climatic Effects,* Williamsburg (Virginia), 28–30 March 1983.

Whitby, K. T., and K. Willeke, 1979: Single optical counters: Principle and field use. aerosol measurements. University Press of Florida, 716 pp.